The Theory and Observation for Ultra-Light Dark Matter

Yi-Fu Cai, Shiyun Lu

University of Science and Technology of China

October 21, 2022

Overview

Table of Contents

Introduction: Why we need Dark Matter

Dark Matter particle interacts neglectably with Standard Model particles, except through gravity.
Observational evidences:

- Cosmological ladder measurements (namely, CMB, SNIa, etc.) determine Ω_{DM};
- Galaxy dynamics (namely, rotation curves, filaments, etc.);
- Gravitational lensing effects (namely, weak-, micro-, etc.);
- Bullet cluster collision; ...

Introduction: Dark Matter Models

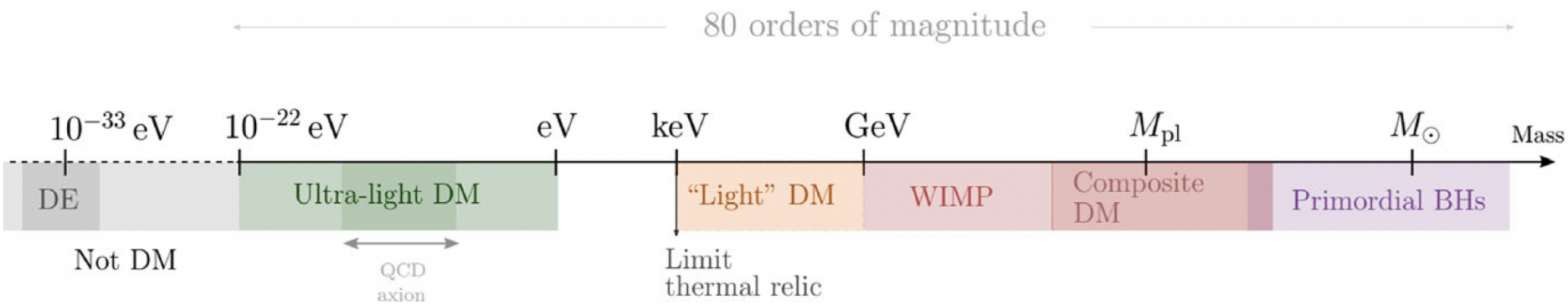

Figure: DM models at different mass scales.

- Ultra-light DM: Ultra-light particles (mostly bosons) with masses of 10^{-24}eV $\sim$ eV.
- WIMP (Weakly interacting massive particle): Massive particle with weakly self-interaction.

Most evidences are from gravitational effects at large scales, leaving the nature of DM unclear.
DM models show different behaviours at small scales.

Table of Contents

Introduction: Cold DM (CDM)

DM model for ΛCDM is a perfect fluid with $\omega \approx 0$ and sound speed $c_s \approx 0$.

ΛCDM model is successful in interpreting the cosmological evolution and compatible with observations at large scales, but is challenged by observations at small scales.

- Core-cusp problem
- Missing satellites (or "Too big to fail" problem)
- Scaling relations

Thus, one expects more DM models which behave as CDM on large scales, while have different small-scale behaviors.

Introduction: non-CDM at smal scales

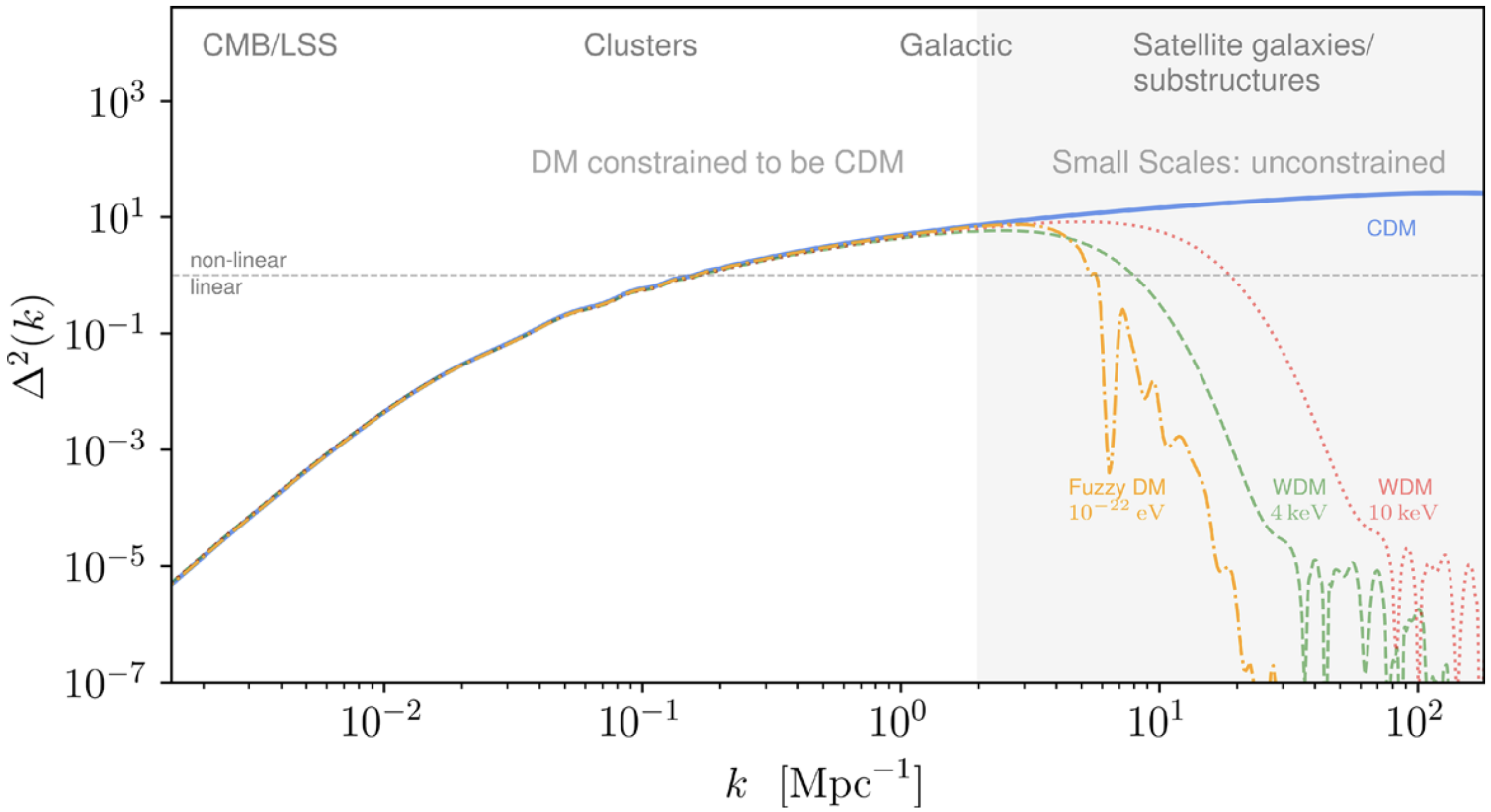

Figure: The dimensionless power spectra by ΛCDM and other DM models.

We can see that non-CDM models predict suppressed power spectra on small scales.

Introduction: Core-cusp problem

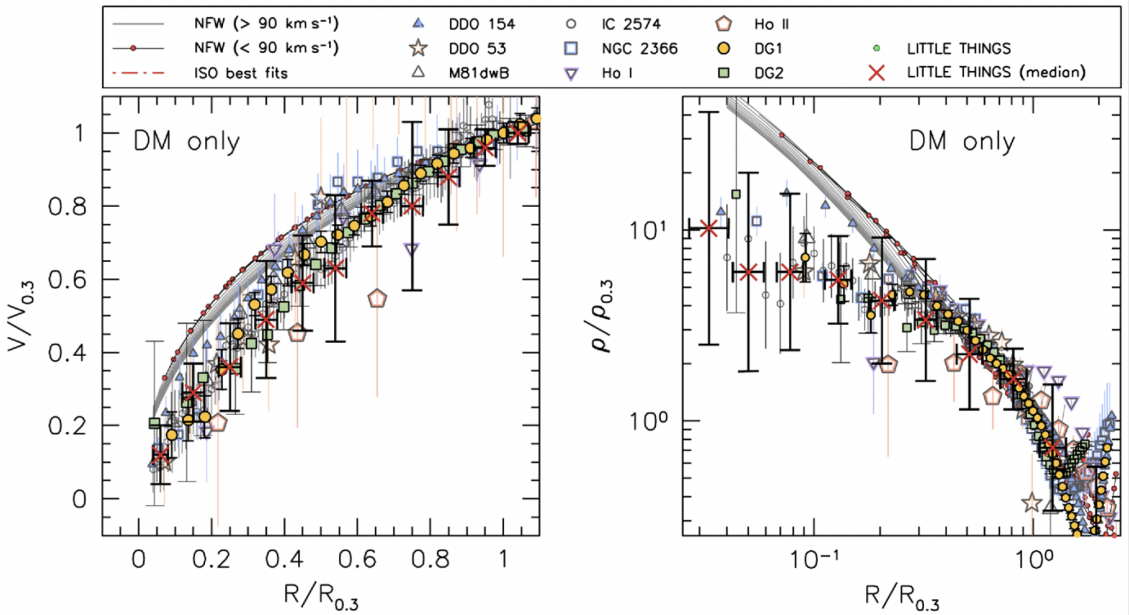

Figure: The observation prefers a core rather than cusp. The plots show the rotation curve and density-radius relation, respectively.

DM halos from numerical simulations generally give a mass profile as NFW profile

$$\rho_{\rm NFW}(r) = \frac{\rho_{\rm s}}{(r/r_{\rm s})\ (1+r/r_{\rm s})^2} \to \begin{cases} 1/r\,, & \text{for } r \ll r_{\rm s} \\ 1/r^3\,, & \text{for } r \gg r_{\rm s} \end{cases} \tag{1}$$

with a divergence at the center $r \to 0$, showing a cusp. While observation prefers a core.

Introduction: Missing satellites (too big to fail)

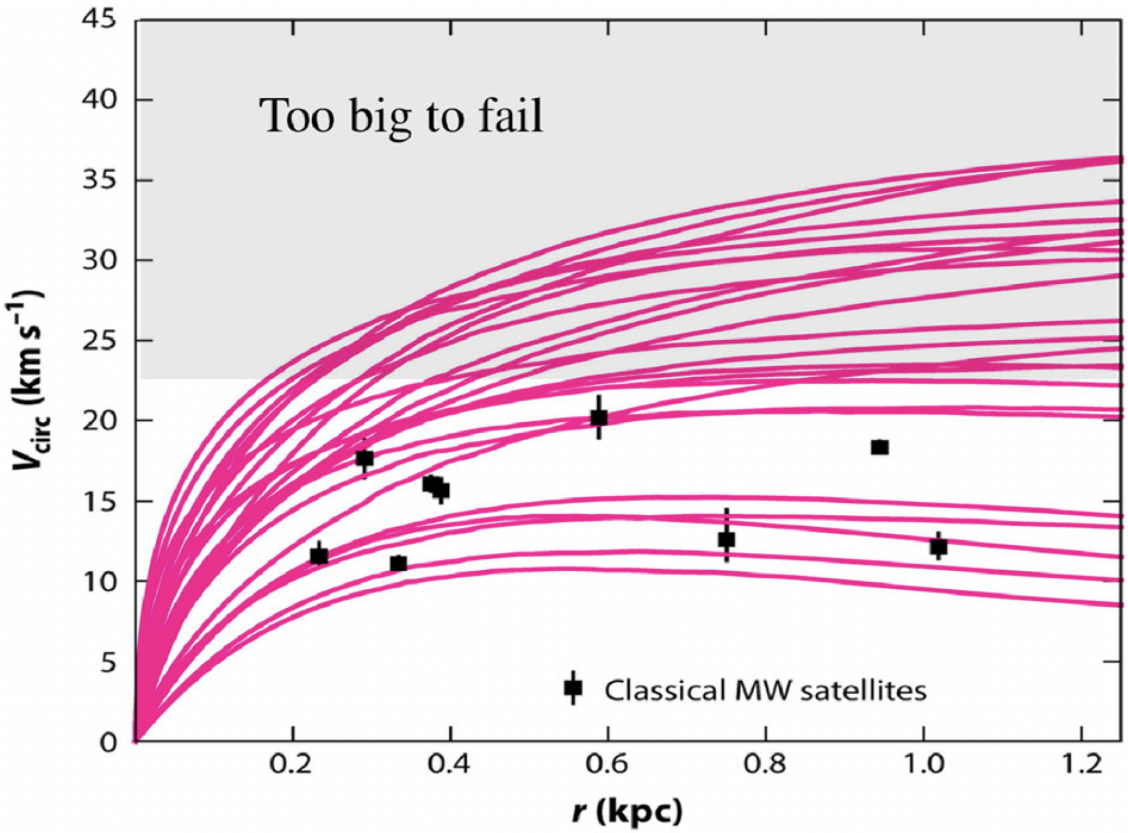

Figure: To interpret the missing satellites in the regime of CDM prediction, we need to imagine the most massive subhalos are too large to fail to form stars and galaxies.

CDM simulation: low-mass halos (below $\sim 10^8 M_\odot$) are highly created, simulation predicts hundreds of subhalos, while galaxy satellites discovered are much less.

Introduction: Scaling relations

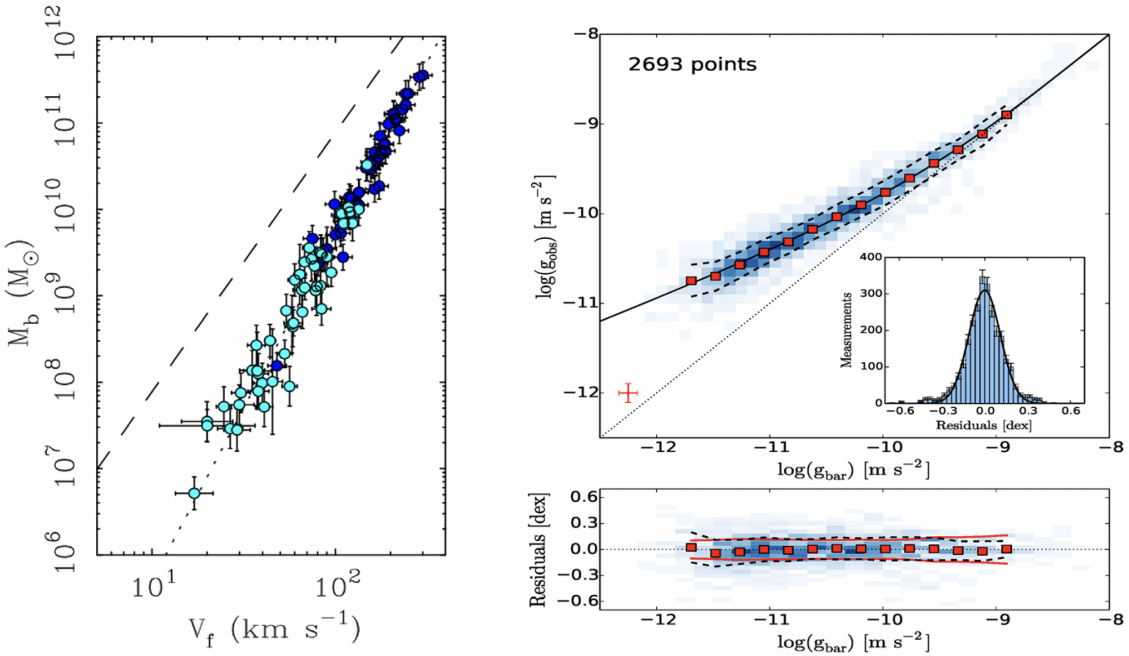

Figure: The Baryonic Tully-Fisher Relation (BTFR) relates the total baryon mass to the asymptotic circular volecity. The dashed line represents the prediction of ΛCDM (with slope 3), while the dotted line fits the data (with slope 4).

Table of Contents

Introduction: ULDM

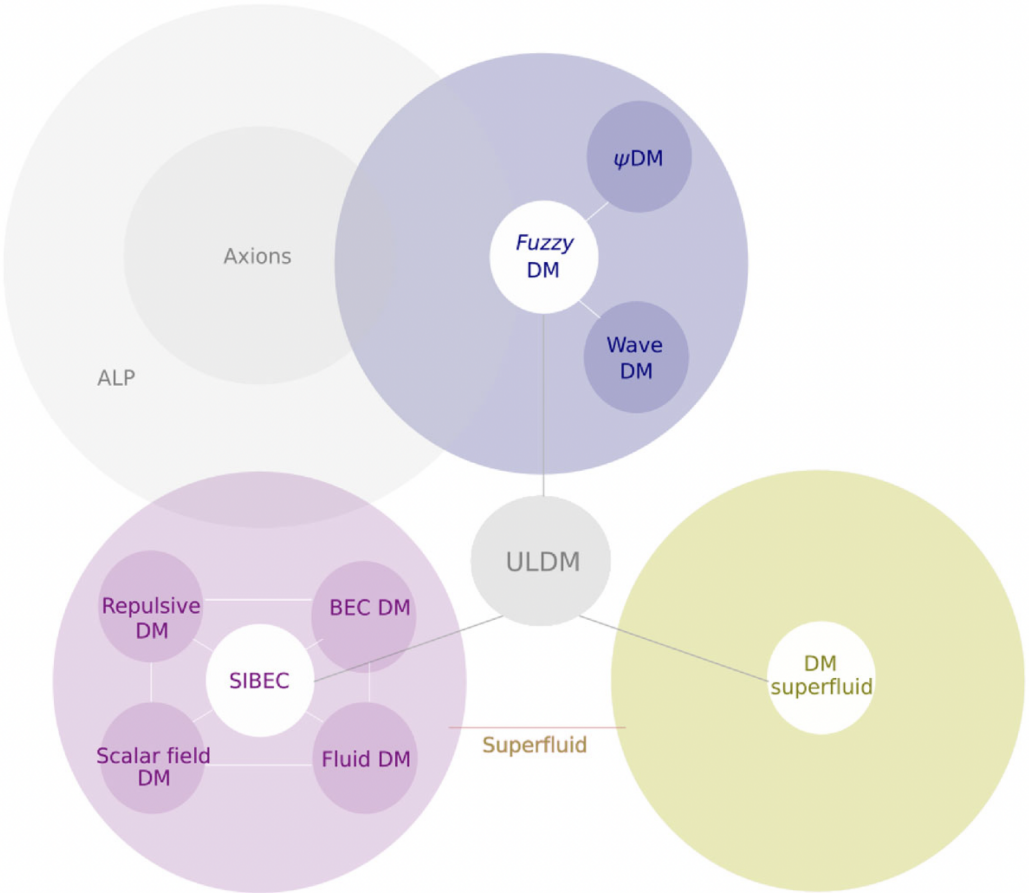

- Ultra-light DM can provide rich phenomenons on small scales.
  Featured on small mass, wave nature, condensate structure.
- Axion models (and ALPs) can produce FDM.
- Fuzzy DM (FDM): gravitational attraction v.s. quantum pressure.
- Self-Interacting FDM (SIFDM):
  The self-interaction can make superfluidity upon condensation.

Table of Contents

(SI)FDM: The action

ULDM minimally coupled to gravity. The action for (SI)FDM

$$S = S_{EH} + S_{\phi} = \int d^4x\sqrt{-g}\left[\frac{R}{16\pi G} + \frac{1}{2}g^{\mu\nu}\partial_\mu\phi\partial_\nu\phi - \frac{1}{2}m^2\phi^2 - \frac{g}{4!}\phi^4\right] , \qquad (2)$$

when $g < 0$ attractive self-interaction, while when $g > 0$ repulsive.

A natural modelling of FDM is **axion**. For axion constituting FDM, $m = \Lambda_a^2/f_a$ and $g = -\Lambda_a^4/f_a^4 < 0$.

FDM: Axion Models

Through an added complex PQ scalar field Φ, the axion field χ is introduced as its complex angle when PQ symmetry is broken.

$$U(\Phi) = \lambda(|\Phi|^2 - f_a^2)^2 \ , \tag{3}$$

An axion potential $V(\chi)$ produced by non-perturbative effects can naturally set a zero total θ-vacua

$$V(\chi) = \Lambda_a^4(1 - \cos(\mathcal{N}_{\mathrm{DW}}\chi/f_a)) \ . \tag{4}$$

The interactions of axions with particles are generally of the form,

$$\frac{g_{\chi\psi}}{2m_\psi}\partial_\mu\chi(\bar{\psi}\gamma^\mu\gamma_5\psi) \ , \tag{5}$$

for the fermion ψ, and

$$-\frac{1}{4}g_{\chi Z}\chi F_{\mu\nu}\tilde{F}^{\mu\nu} \ , \tag{6}$$

for the boson Z. For example, QCD axions couple to photons with

$$g_{\chi\gamma} = \frac{\alpha_{\mathrm{EM}}}{2\pi f_a}\mathcal{N}_{DW}c_{\chi\gamma} \ , \tag{7}$$

FDM: Axions Constituting DM

Axion during Inflation

If $f_a \lesssim H_I/2\pi$, PQ symmetry is broken after inflation and then we can take average of all patches

$$\langle \chi_i^2 \rangle = f_a^2 \pi^2/3 \ , \tag{8}$$

If $f_a \gtrsim H_I/2\pi$, PQ symmetry is broken during inflation and then in our patch universe within horizon there is

$$\langle \chi_i^2 \rangle = f_a^2 \theta_i^2 + \langle \delta\chi^2 \rangle \ , \tag{9}$$

FDM: Axions Constituting DM

Background evolution after inflation

When the misalignment angle is small $\chi/f_a = \theta_a \ll 1$,

$$\ddot{\chi}_0 + (3H + \Gamma)\dot{\chi}_0 + m_a^2 \chi_0 = 0 \ . \tag{10}$$

We can see that

- When $H \gg m_a$, the χ_0 background rolls down with a very slow $\dot{\chi}_0 \simeq -\frac{m_a^2}{3H}\chi_0$. Under this condition, $\omega_a \simeq -1$.
- When $H \approx m_a$, the axion background begins oscillating.
- Some time after oscillation begins, $H \ll m_a$, and $\rho_a \sim a^{-3}$.

FDM: Axions Constituting DM

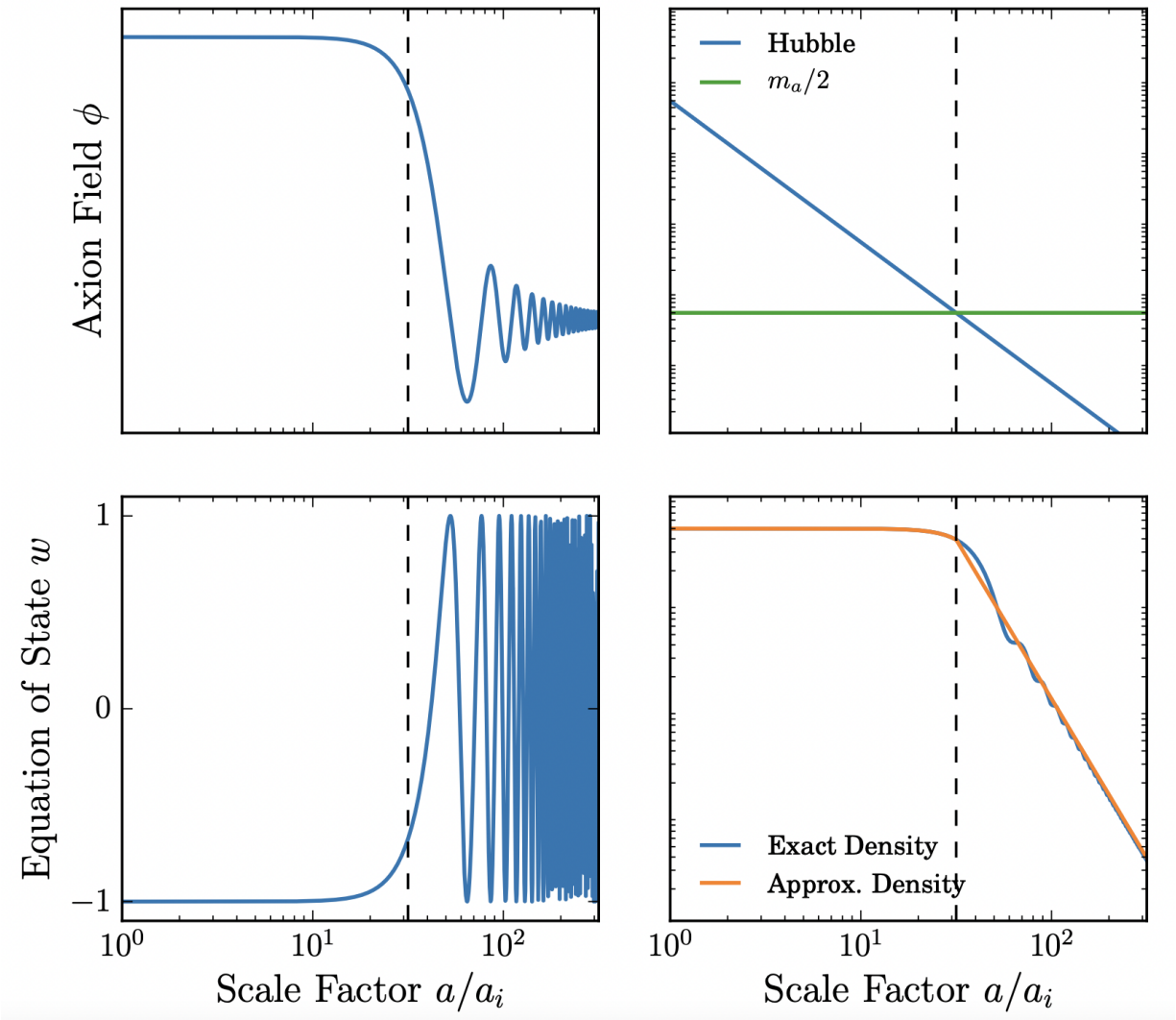

Figure: Background evolution for the ALP model in a RD universe.

FDM: Axions Constituting DM

DM Production of ALPs

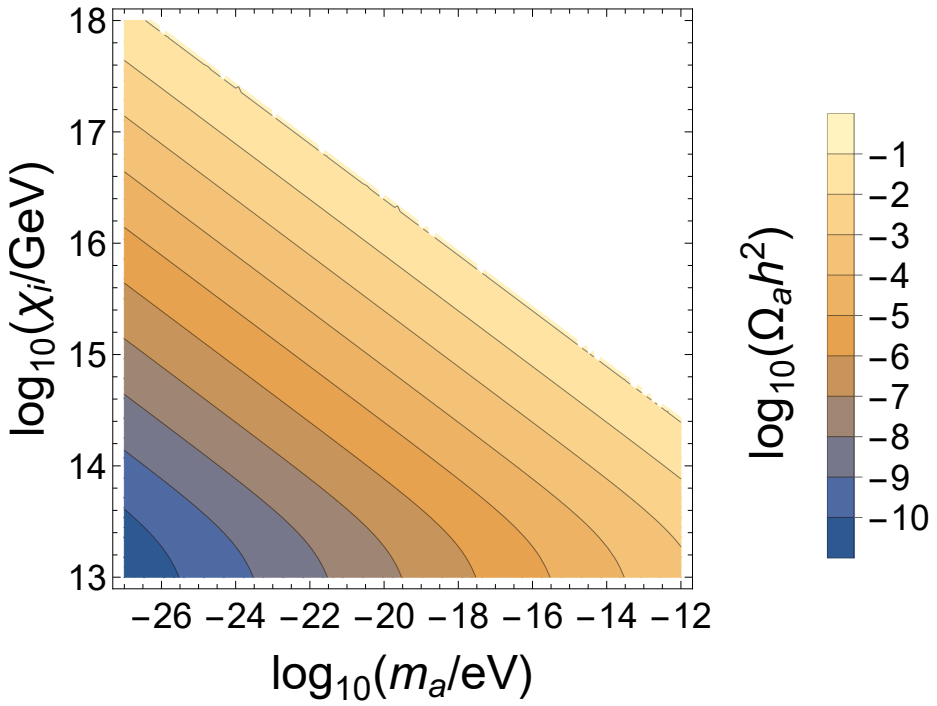

Figure: Relic density of ALP dark matter produced through misalignment

ALP DM relic density, when the ALP oscillated during different epoches

$$\Omega_a \approx \begin{cases} \frac{1}{6}(A^2\Omega_r)^{3/4}(m_a/H_0)^{1/2}\langle\chi_i^2/M_{\mathrm{pl}}^2\rangle & a_{\mathrm{osc}} < a_{\mathrm{eq}} \\ \frac{1}{6}A^2\Omega_m\langle\chi_i^2/M_{\mathrm{pl}}^2\rangle & a_{\mathrm{eq}} < a_{\mathrm{osc}} \lesssim 1 \\ \frac{1}{6}(m_a/H_0)^2\langle\chi_i^2/M_{\mathrm{pl}}^2\rangle & a_{\mathrm{osc}} \gtrsim 1 \end{cases} . \quad (11)$$

FDM: Perturbations Evolution

Next, we study a general case for FDM. The oscillation behavior is similar to axion and can constitue DM. We check the difference of FDM from CDM, although the averaged ω of FDM is also 0.
In comoving gauge, the evolution of perturbations

$$\ddot{\delta} + 2H\dot{\delta} - 4\pi G\rho\,\delta + \frac{k^2}{a^2}\frac{\delta p}{\rho} = \ddot{\delta} + 2H\dot{\delta} + \left(\frac{k^2}{a^2}c_s^2 - 4\pi G\rho\right)\delta = 0\,, \tag{12}$$

where $\delta = \delta\rho/\rho$, and we get the dispersion relation $\omega_k^2 = \frac{k^2}{a^2}c_s^2 - 4\pi G\rho$. Assuming an ansatz $\delta\phi = \delta\phi_+ \sin(mt) + \delta\phi_- \cos(mt)$, we get the expression for sound speed

$$c_s^2 = \frac{k^2}{4m^2a^2}\left(\frac{1}{1+\frac{k^2}{4m^2a^2}}\right). \tag{13}$$

The Jeans scale k_J defined by $\omega_k(k_J) = 0$.
For modes with $\lambda < \lambda_J$, $\omega_k^2 > 0$, and the perturbations oscillate.
For modes with $\lambda > \lambda_J$, $\omega_k^2 < 0$, and the perturbations grow.

FDM: Evolution on small scales

We are interested in the behaviour of DM in galaxies, when $H \ll m$ and in the non-relativistic limit.
In the Newtonian gauge, we can rewrite the ULDM action

$$S_\phi = \int \mathrm{d}^4x\, a^3 \left[\frac{1}{2}(1-4\Phi)\,\dot{\phi}^2 - \frac{1}{a^2}(\partial_i\phi)^2 - (1-2\Phi)V(\phi)\right], \tag{14}$$

rewrite the field as

$$\phi = \frac{1}{\sqrt{2ma^3}}\left(\psi\, e^{-imt} + \psi^*\, e^{imt}\right), \tag{15}$$

we get the Schrdinger-Possion system of equations

Fuzzy DM vs SIFDM

$$\begin{cases} i\dot{\psi} = -\dfrac{1}{2m}\nabla^2\psi + m\,\Phi\,\psi + \dfrac{g}{8m^2}\,|\psi|^2\psi + \dfrac{g_3}{12m^3}\,|\psi|^4\psi + \cdots \\ \nabla^2\Phi = 4\pi G\,(\rho - \bar{\rho}) \end{cases} \Longrightarrow \begin{cases} g_i = 0 & \text{Fuzzy DM} \\ g_i \neq 0 & \text{SIFDM} \end{cases} \tag{16}$$

FDM: Evolution on small scales

We can also rewrite the above equations in a hydrodynamical-like form by defining

$$\psi \equiv \sqrt{\frac{\rho}{m}} e^{i\theta} \ , \quad \mathbf{v} \equiv \frac{1}{am} \nabla \theta \ . \tag{17}$$

and get the Madelung equations

$$\begin{aligned} &\dot{\rho} + 3H\rho + \frac{1}{a} \nabla \cdot (\rho \mathbf{v}) = 0 \, , \\ &\dot{\mathbf{v}} + H\mathbf{v} + \frac{1}{a} (\mathbf{v} \cdot \nabla) \mathbf{v} = -\frac{1}{a} \nabla \Phi + \frac{\nabla P_{\rm int}}{\rho} + \frac{1}{2a^3 m^2} \nabla \left(\frac{\nabla^2 \sqrt{\rho}}{\sqrt{\rho}} \right) . \end{aligned} \tag{18}$$

where the $P_{\rm int}$ is the pressure from the self-interactions, $P_{\rm int} \propto \rho^{(j+1)/j}$ with $j = 1$ for two-body interaction, and the last term is the "quantum pressure".
For FDM model, the quantum pressure can prevent the DM from clustering or collapsing, naturally form a cored profile inside the condensate region.
We can naively estimate the scale when the non-CDM behavior take effect, as $\lambda < \lambda_{\rm dB}$.
The de Brogile wavelength for a MW-like galaxy

$$\lambda_{\rm dB} \simeq 0.2 \left(\frac{m}{10^{-22}\,{\rm eV}} \right)^{-1} \left(\frac{V_{200}}{v} \right) {\rm kpc} \ . \tag{19}$$

SIFDM: Evolution on small scales

For SIFDM, we need to consider the self-interaction term, and the dispersion relation changes to

$$\omega_k^2 = \frac{g n_0}{4m^2}\frac{k^2}{2m} + \frac{k^4}{4m^2} \ , \tag{20}$$

where n_0 is the number density of particles, and the two competing terms switch their domination when

$$k_*^2 = \frac{|g| n_0}{2m} \ , \tag{21}$$

which determines the wavelength $\lambda_* = 2\pi/k_*$. The λ_* is proportional to the healing length $\xi = \hbar/\sqrt{2mgn}$. Then we get the conditions for stable solutions

$$\begin{aligned}
g > 0 \quad &\longrightarrow \quad \forall\lambda \qquad \text{Solution oscillates. Condensate (long range)} \\
g < 0 \quad &\longrightarrow \begin{cases} \lambda > \lambda_* & \text{Structures grow. No condensate.} \\ \lambda < \lambda_* & \text{Solution oscillates. Condensate (finite size)} \end{cases}
\end{aligned} \tag{22}$$

note that SIFDM with repulsive interaction is a superfluid, while for the attractive case, the stable solution is not a BEC superfluid, but a soliton.

Table of Contents

FDM observations: linear suppression of power spectrum

For FDM model, the structure formation suffers a cutoff on Jeans scale k_J.
The modification of power spectrum can be evaluated

$$P_{\rm FDM}(k,z) = T^2_{\rm FDM}(k,z)\, P_{\Lambda{\rm CDM}}(k,z) = T^2_{\rm FDM}(k,z) \left(\frac{D(z)}{D(0)}\right)^2 P_{\Lambda{\rm CDM}}(k)\,, \tag{23}$$

where $D(z)$ is the growth factor that depends on the expanding history of the universe.
The FDM transfer function is

$$T_{\rm FDM} = \frac{\cos(x^3_{{\rm J}(k)})}{1 + x^8_{\rm J}(k)}\,, \tag{24}$$

where

$$x_{\rm J}(k) = 1.61 \left(\frac{m}{10^{-22}\,{\rm eV}}\right)^{1/18} \left(\frac{k}{k_{\rm J,eq}}\right), \quad k_{\rm J,eq} = 9 \left(\frac{m}{10^{-22}\,{\rm eV}}\right)^{1/2} {\rm Mpc}^{-1}\,. \tag{25}$$

We can constrain FDM from the CMB and LSS data, and also on even smaller scale such as Ly-α forest or 21-cm lines.

FDM observations: suppression of FDM halo formation

The suppression of power spectrum also induce a suppression of FDM halo formation.
An estimation of the smallest mass of halos able to form

$$M_{\rm lin} = \frac{4\pi}{3} R_{1/2,\rm lin} \langle \rho_{\rm FDM} \rangle = 4 \times 10^{10} M_\odot \left(\frac{m}{10^{-22}\,\rm eV} \right)^3 \left(\frac{\Omega_m}{0.3} \right) \left(\frac{h}{0.7} \right)^2 . \quad (26)$$

FDM predicts a large suppression of halos for $M < 10^{10} M_\odot$ if $m = m_{22}$.

The suppression of power spectrum also suppresses the galaxy formation.
It also suppresses the substructure, which can be probed by gravitational lensing and streams.

FDM observations: CMB and matter power spectrum

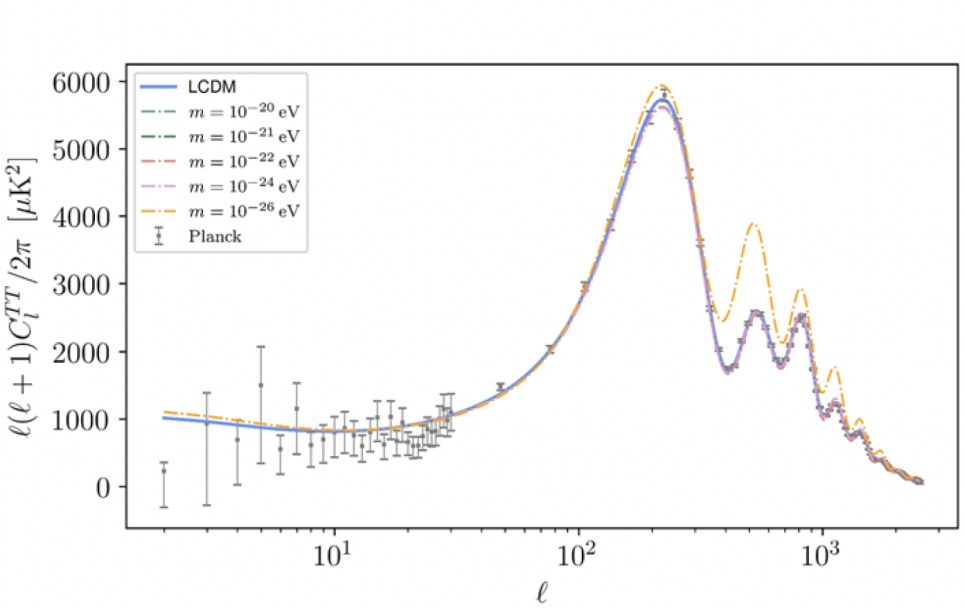

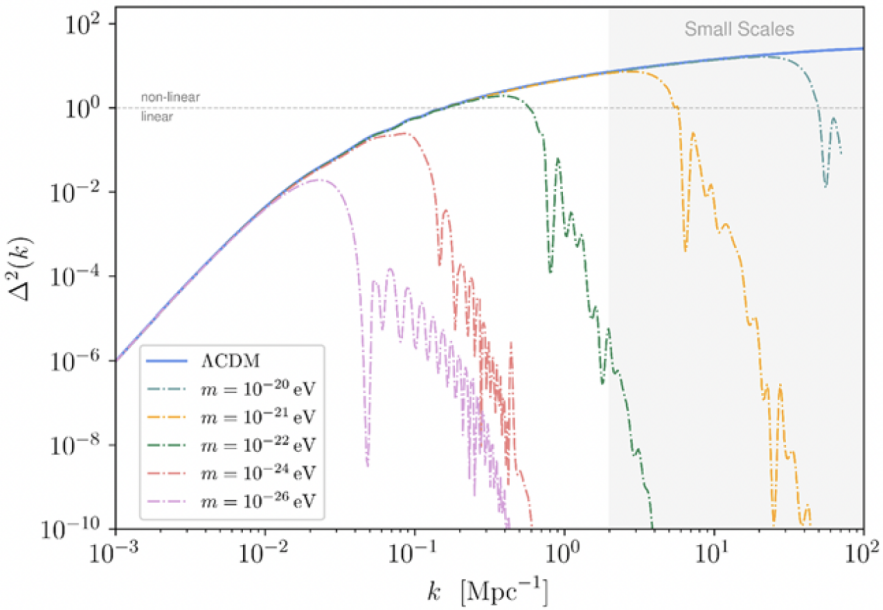

Figure: The angular power spectrum of CMB temperature anisotropy and the matter power spectrum, respectively. We make comparison of FDM with ΛCDM.

FDM observations: Halo mass function modification

Power spectrum suppression also leads to a modification of the halo mass function (HMF). The HMF can be fit using simulation

$$\left(\frac{\mathrm{d}n}{\mathrm{d}M}\right)_{\mathrm{FDM}} = \left[1 + \left(\frac{M}{M_0}\right)^{-1.1}\right]^{-2.2} \left(\frac{\mathrm{d}n}{\mathrm{d}M}\right)_{\mathrm{CDM}} . \tag{27}$$

and another HMF is obtained using different methods

$$\left(\frac{\mathrm{d}n}{\mathrm{d}M}\right)_{\mathrm{FDM}} = -\frac{\rho_m}{M} f(\nu) \frac{\mathrm{d}\ln\sigma^2}{\mathrm{d}\ln M} . \tag{28}$$

where $\nu \equiv \delta_c/\sigma$, $\sigma(M)$ is the variance of the power spectrum, and δ_c is the critical collapse overdensity. Function $f(\nu)$ comes from Sheth-Thormen model.

The probe sensitive to the low-mass end of HMF can be used to test FDM, e.g. luminosity function of galaxies, and reionization history.

FDM observations: Sub-halo mass function suppression

A fitting form of FDM sub-halo mass function

$$\left(\frac{\mathrm{d}n_{\mathrm{sub}}}{\mathrm{d}\ln M}\right)_{\mathrm{FDM}} = f_1(M) + f_2(M)\left(\frac{\mathrm{d}n_{\mathrm{sub}}}{\mathrm{d}\ln M}\right)_{\mathrm{CDM}}, \tag{29}$$

where

$$f_1(M) = \beta \exp\left[-\frac{1}{\sigma}\left(\ln\frac{M}{M_1 \times 10^8\, M_\odot}\right)^2\right],$$
$$f_2(M) = \left[1 + \left(\frac{M}{M_2 \times 10^8\, M_\odot}\right)^{-\alpha_1}\right]^{-10/\alpha_1}. \tag{30}$$

We use the CDM sub-halo mass function

$$\left(\frac{\mathrm{d}n_{\mathrm{sub}}}{\mathrm{d}\ln M}\right)_{\mathrm{CDM}} = a_{\mathrm{CDM}}\left(\frac{M}{10^8\, M_\odot}\right)^{-\alpha_0}. \tag{31}$$

FDM observations: Sub-halo mass function suppression

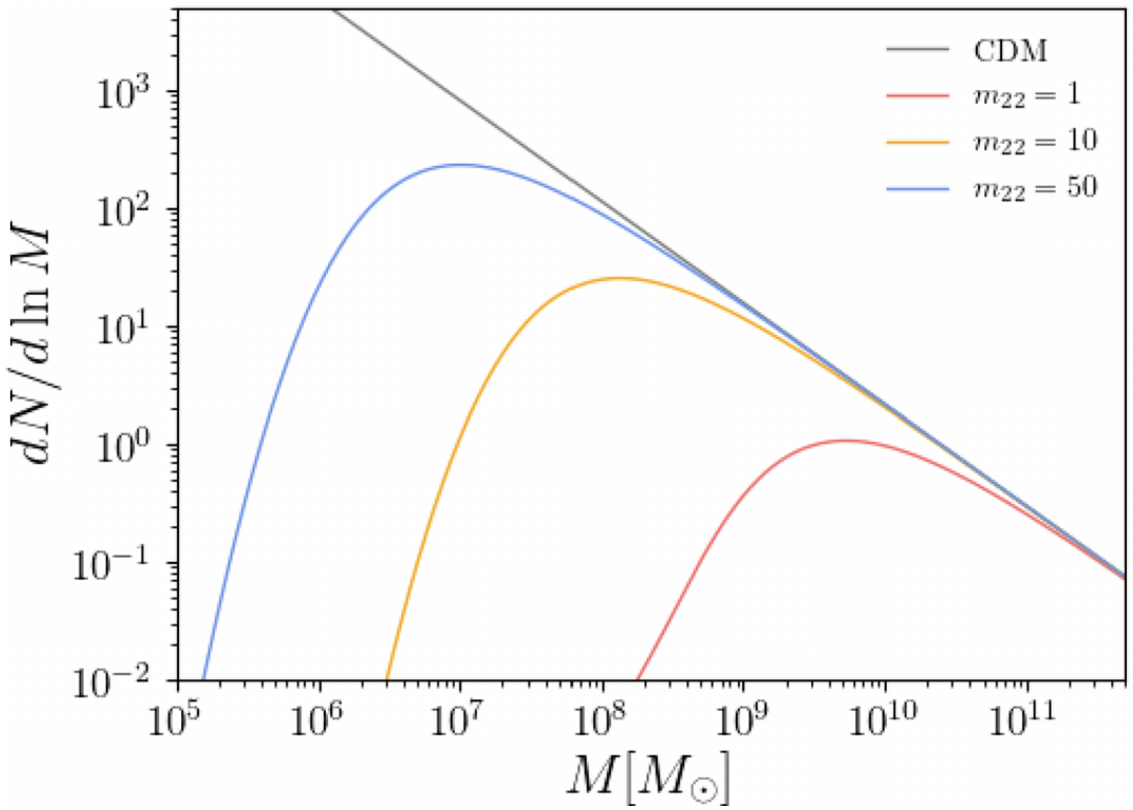

Figure: Comparison of the sub-halo mass function from FDM and CDM.

FDM observations: The central core

We have seen that ULDM can form a stable area in the center of a galaxy, as a soliton (or a Bose star for FDM). The soliton raduis of MW-like mass

$$r_c \simeq 0.16 \left(\frac{m}{10^{-22}\,\mathrm{eV}}\right)^{-1} \left(\frac{M}{10^{12}\,M_\odot}\right)^{-1/3} \mathrm{kpc} \,. \tag{32}$$

so the density profile is changed to

$$\rho_{\mathrm{halo}} \simeq \begin{cases} \rho_c & \text{for } r \leq r_c \\ \rho_{\mathrm{NFW}} & \text{for } r > r_c \end{cases} . \tag{33}$$

with a central core instead of a cusp.

FDM observations: Dynamical effects

The dynamical effects arise because of the wave-like behavior of ULDM inside the soliton core.
The relaxation between FDM and macroscopic objects.
These effects can lead to heating, cooling or dynamical friction of the macroscopic object.

- Gravitational heating. This leads to an increase in the dispersion relation of the star, expanding the stellar system.
- Modified dynamical friction. Some puzzles can potentially be explained.

FDM observations: Solving problems

We can see how ULDM can solve the problems

- Core-cusp. The central core by soliton changes the DM halo density profile.
- Missing satellite. The lower bound of the FDM halo masses.
- ...

The preferred FDM solving the problems coincidentally has a typical mass of $m \sim 10^{-22}$ eV. BUT, it doesn't mean that all FDM have to stay around this mass scale.

Table of Contents

Observational constraints

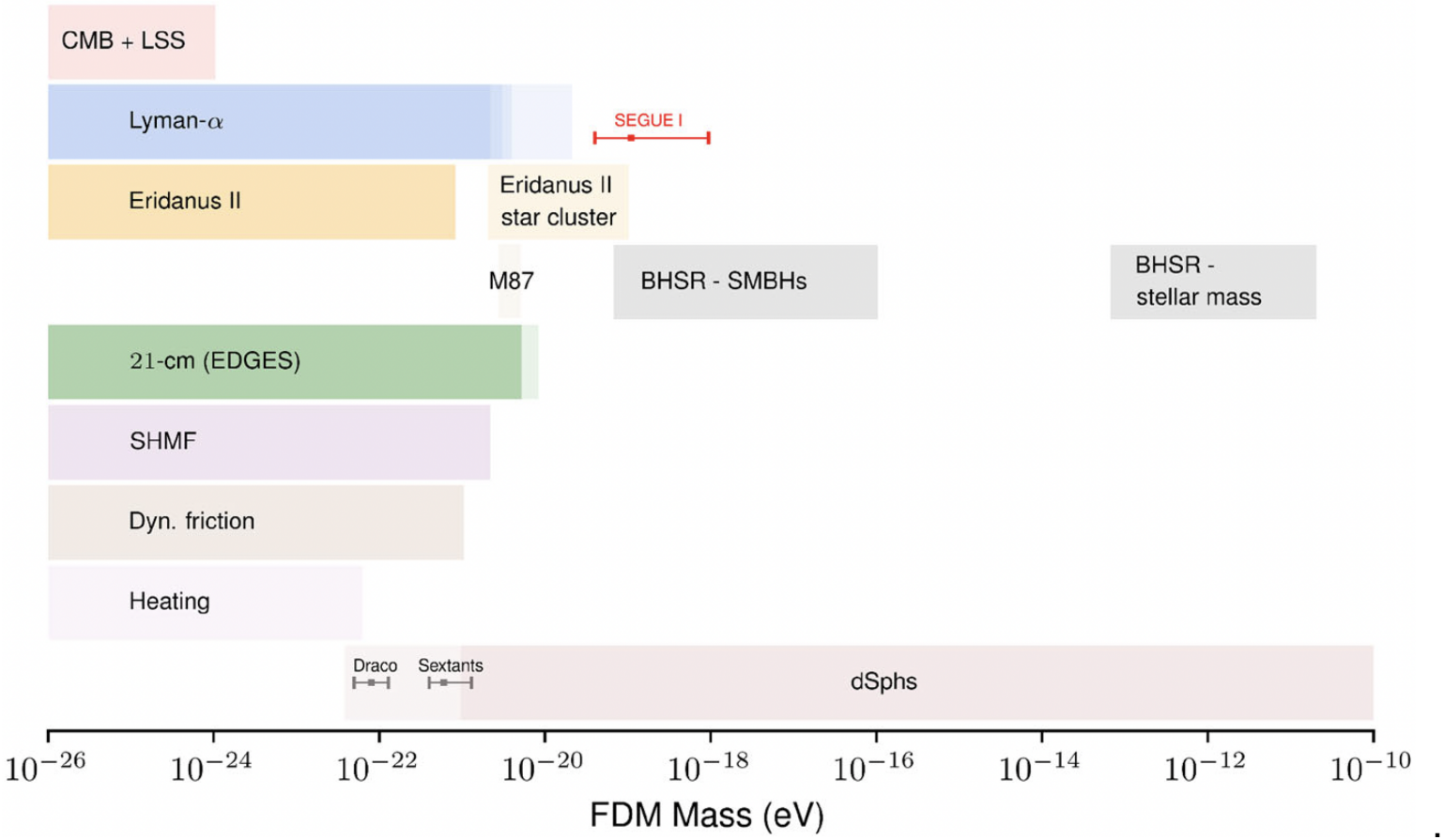

Figure: The mass range of FDM constrained by observations, assuming FDM constitute most of the DM.

Observational constraints

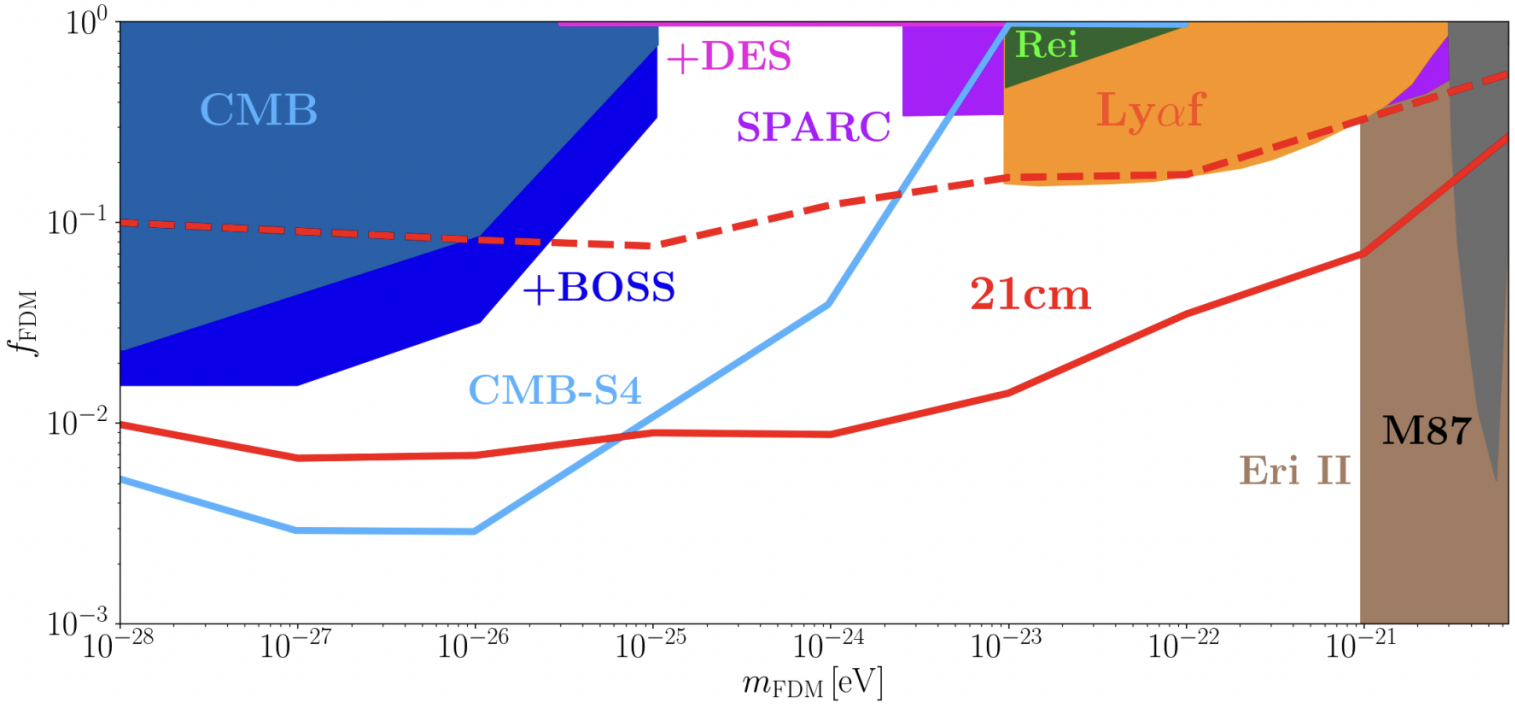

Figure: The parameter space of FDM constrained and to be constrained by observations. Plot taken from 2207.05083.

Table of Contents

Observational constraints: CMB

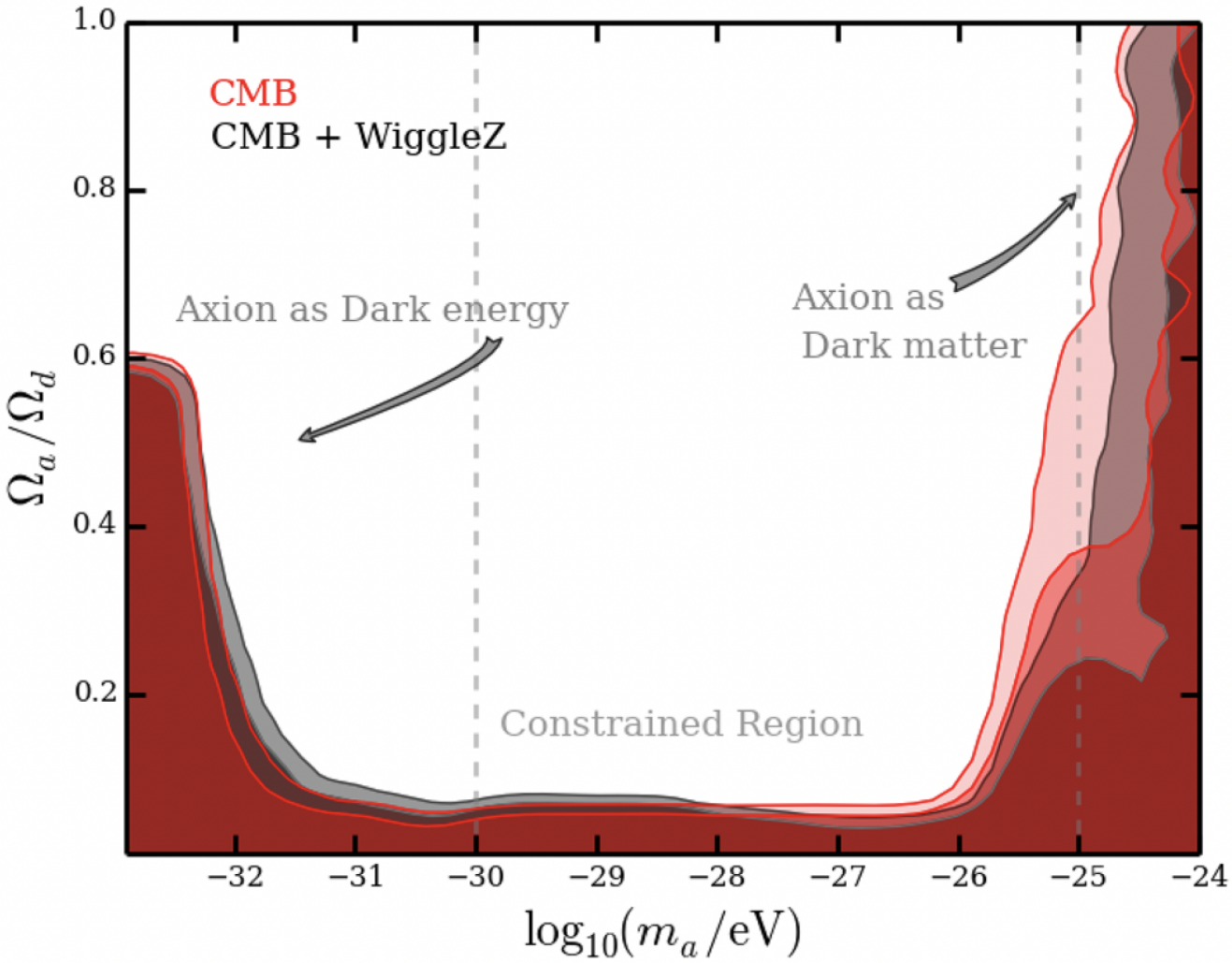

Figure: The 2σ and 3σ of the ultra-light fraction of DM. Red regions show the CMB-only constriant, and grey regions constriants also include LSS data.

Observational constraints: Lyman-α

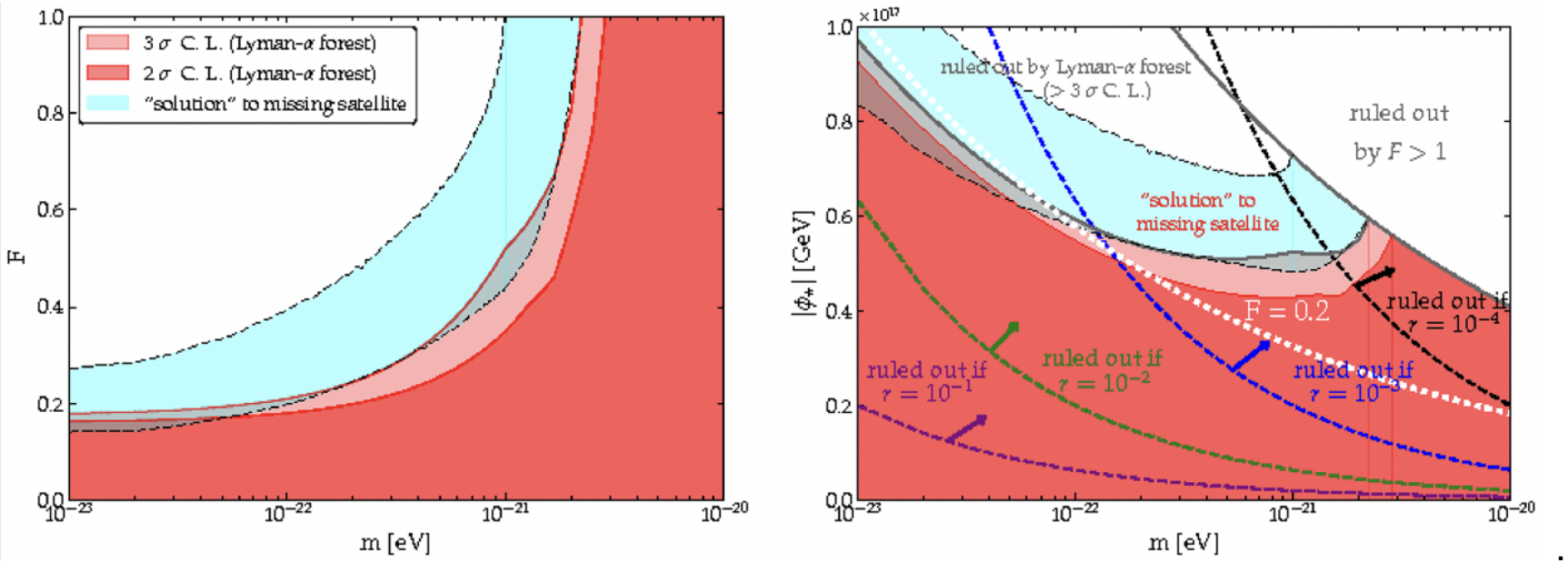

Figure: Left: The FDM fraction as function of FDM particle mass, constrained by Ly-α forest data. Right: The value of the displaced field. r is the tensor-to-scalar ratio.

Observational constraints: 21 cm HI signal

The suppression of FDM power spectrum is on small scale, can be probed by CMB, LSS, and Ly-α.
21 cm HI signal can probe even smaller scale, however, it is hard to distangle astrophysical effects on such scales.
Future probe can provide more information on astropysical processes.

Global 21 cm signal by EDGES put bounds on FDM:

- (1805.01253) $m \geq 5 \times 10^{-21}$ eV.

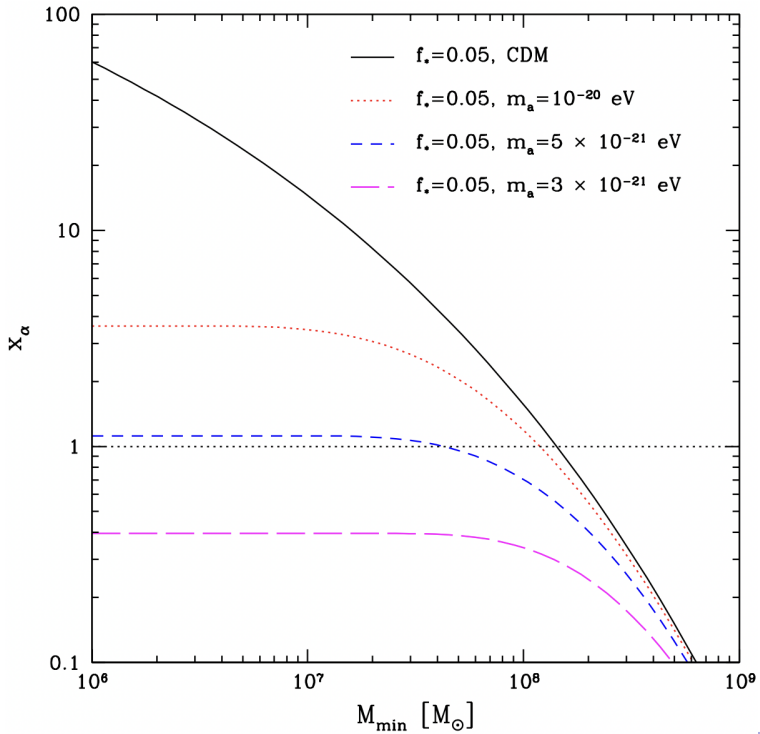

Observational constraints: DES combined to CMB

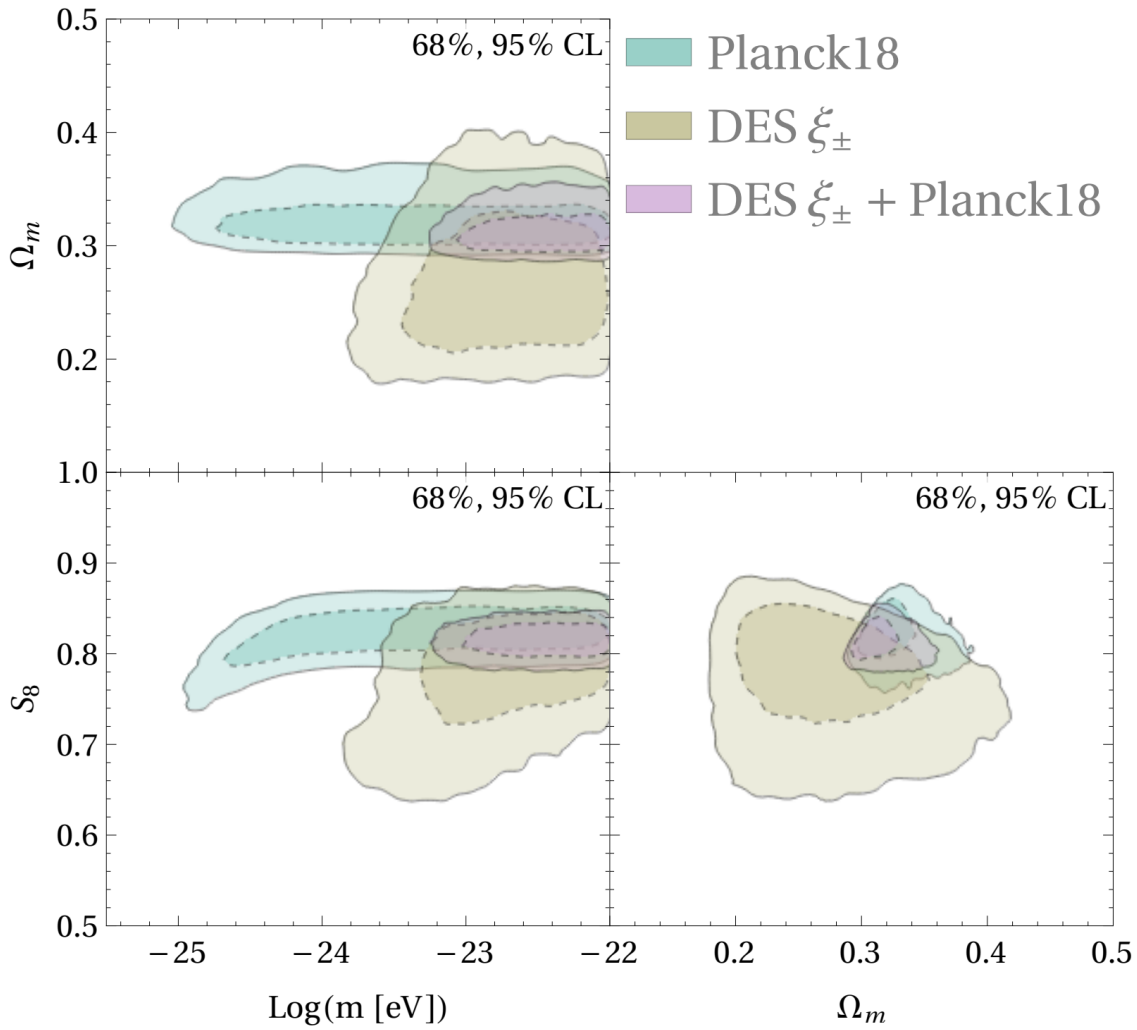

Figure: The constraint of FDM mass from Dark Energy Survey-Year 1, combined with Planck data. Plot is taken from 2111.01199.

Table of Contents

Observational constraints: local MW

Observations of the MW and Local group like: Gaia, LSST, PFS, WFIRST

- Gaia. Scales much smaller than the virial radius.
- PFS. Complementing Gaia's survey.
- LSST. Expected on scales close to $R_{\rm vir}$.

We can get information of inner structure of halos, satellites distributions, and gravitational potential on even larger scales.
They can be used to probe the three classes of ULDM effects as discussed above: power spectrum suppression, core structure and dynamical effects.

Dwarf galaxy. e.g. Eridanus-II.

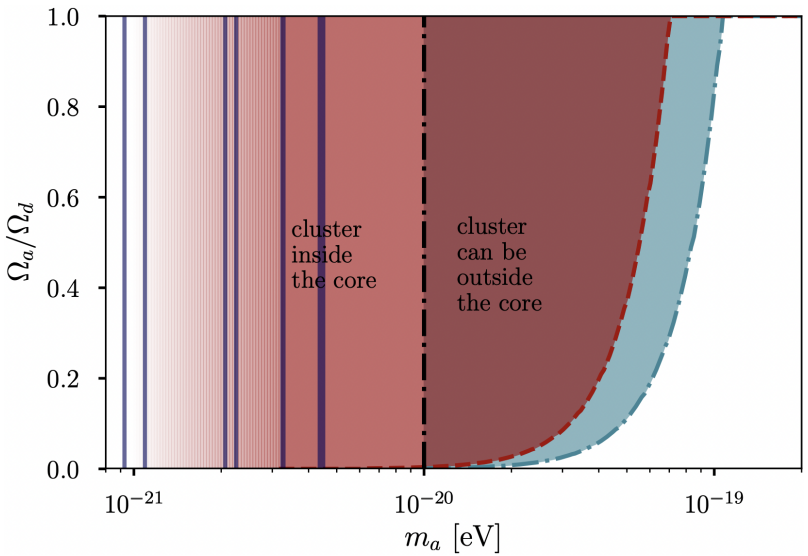

Figure: The constriant for FDM by the existence and survival of Eri II star cluster. Plot taken from 1810.08543.

Observational constraints: substructure probes

Stellar streams:
Initially cold and very sensitive to gravitational potential. So sensitive to DM substructure, and can cause dynamical heating.
Potentially test DM model in future.

Strong lensing:
Substructure can modify the lensed images of quasar, including changing morphology and flux ratio.
Strong lensing is importatnt probe for signatures in substructures, like vortices and dark disks.

Probes sensitive to gravitational potential can also test sub-halo mass function of FDM model. An FDM mass bound obtained in this way $m \sim 2.1 \times 10^{-21}$ eV.

Observational constraints: UV luminosity function

By comparing the predicted cutoff in luminosity functions, we can also put constriants on FDM mass.

- Hubble Ultra Deep Field (HUDF) for searching galaxies at high-z.
  Using the data from HUDF and the halo mass function simulation in (27), 1508.04621 gives mass bound $m \gtrsim 1.2 \times 10^{-22}$ eV (2σ).

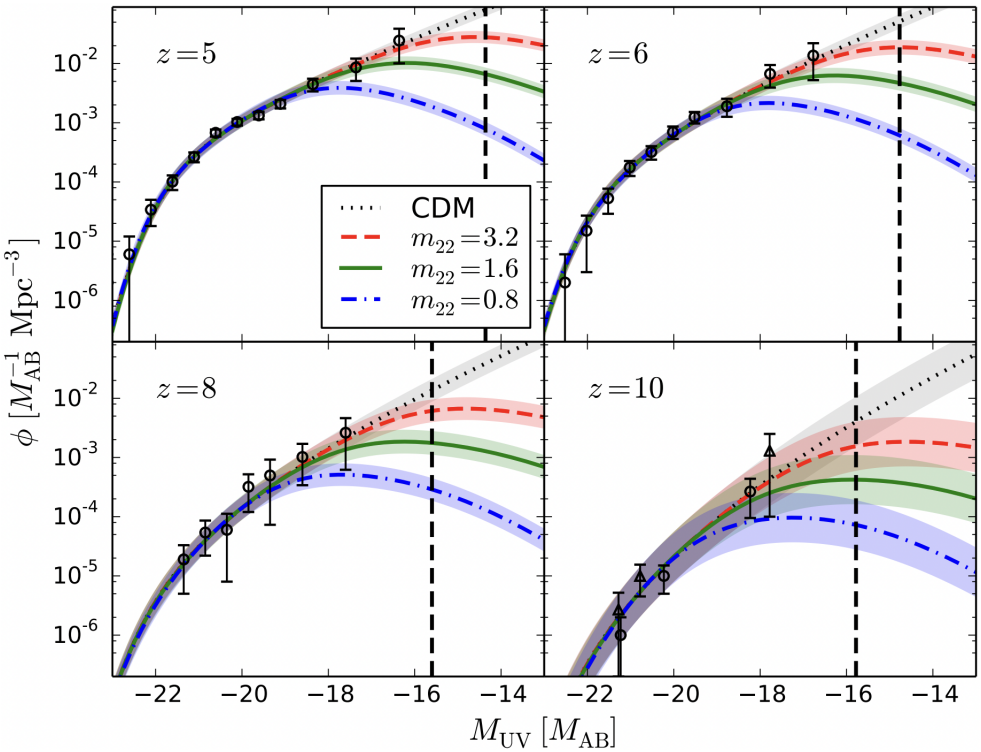

- Deep IRAC (from Spitzer Space Telescope). Can be combined with HUDF data.
- Hubble Frontier Field (HFF) observing gravitational lensed ultra-faint galaxies.

There are plenty works on this, all giving a lower bound for FDM mass around 10^{-22} eV.

Table of Contents

Observational constraints: Black hole superradiance

BHSR: Ultra-light particles can be largely produced around spinning BHs.
An incoming wave can be amplified by the BH under some conditions, forming a "cloud" of ultra-light particle condensate.
Such superradiance depends on BH spin, BH mass and ultra-light particle mass.

A range of ULDM has also be excluded this way.

- For stellar mass BH, a work excludes $7 \times 10^{-20}\text{eV} < m < 10^{-16}\text{eV}$.
- Data from EHT on M87* excludes $2.9 \times 10^{-21}\text{eV} < m_s < 4.6 \times 10^{-21}\text{eV}$ for scalar ULDM.

Observational constraints: Wave nature of ULDM

Apart from the consequences of wave nature of ULDM, as discussed above, there is also direct distinguished signatures from the wave nature, like vortices and interferene patterns.

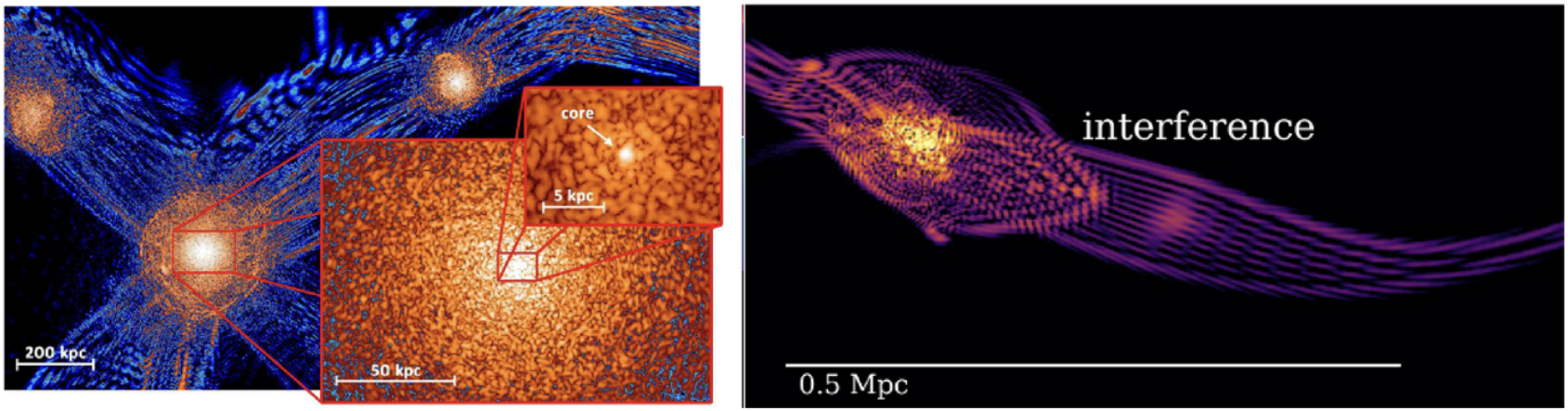

Figure: The interference pattern in DM halos from hydrodynamical simulations of FDM model.

Conclusions

- We have reviewed a class of DM models, and particularly the ULDM models, that can address the issues within ΛCDM.
- We have then introduce the basic idea of ULDM including FDM and extended models with self-interactions.
- We showed that how these ULDM can give new structures at small scales, and produce rich phenomena both in cosmological and astrophysical observations. Meanwhile, the wave nature can hopefully solve the problems in the CDM model.
- We present the constraints from observations for FDM, and showed that, the preferred FDM mass solving problems are seemingly disfavored by some current constraints. We may need more careful works on observations, numerical simulations and theoretical modeling.

The end. Thanks for listening!